Journal of Translational Medicine

RESEARCH

Open Access

# Re-analysis of single cell and spatial transcriptomics data reveals B cell landscape in gastric cancer microenvironment and its potential crosstalk with tumor cells for clinical prognosis

Xing Cai[1,2†], Jinru Yang[1,2,6†], Yusheng Guo[3,4†], Yanchao Yu[5], Chuansheng Zheng[3,4*] and Xiaofang Dai[1,2*]

## Abstract

**Background** At present, immunotherapy has become a powerful treatment for advanced gastric cancer (AGC), but not all patients can benefit from it. According to the latest research, the impact of B cell subpopulations on the immune microenvironment of gastric cancer (GC) is unknown. Exploring whether the interaction between B cells and tumor cells in GC affects the effectiveness of immunotherapy has attracted our interest.

**Methods** This study involved the re-analysis of single-cell RNA (scRNA) and spatial transcriptomics (ST) data from publicly available datasets. The focus was on investigating the subpopulations and differentiation trajectories of B cells in the gastric cancer (GC) tumor immune microenvironment (TIME). Spatial transcriptomics (ST) and multiple immunofluorescence (mIF) revealed a clear co-localization pattern between B cells and tumor cells. Multiple immunotherapy datasets were collected to identify unique immunotherapy biomarkers. The unique immunotherapeutic potential of targeting CCL28 was validated through a mouse gastric cancer model. In addition, flow cytometry revealed changes in the tumor immune microenvironment targeting CCL28.

**Results** The re-analysis of ST data from multiple cancer types revealed a co-localization pattern between B cells and tumor cells. A significant number of IgA plasma cells were identified in the GC TIME. Five different tumor-infiltrating B cell subpopulations and two unique B cell differentiation trajectories were characterized, along with seven GC-related states. By analyzing the communication between GC cells and B cells, it was further discovered that tumor cells can influence and recruit plasma cells through CCL28-CCR10 signaling. Additionally, there was a crosstalk between GC cells and B cells. Finally, we identified the LAMA/CD44 signaling axis as a potential prognostic marker for immunotherapy through a large amount of immunotherapy data. We also validated through various animal tumor

[†]Xing Cai, Jinru Yang and Yusheng Guo have authors contributed equally to this article.

*Correspondence:
Chuansheng Zheng
hqzcsxh@sina.com
Xiaofang Dai
2003xh1047@hust.edu.cn
Full list of author information is available at the end of the article

models that targeting CCL28 can significantly promote $CD8^+$T cell infiltration and function in the TME by regulating B cell and plasma cell functions, and has the ability to synergize immunotherapy.

**Conclusion** The co-localization and crosstalk between GC cells and B cells significantly affect the efficacy of immunotherapy, and inhibiting the CCL28-CCR10 signal axis is a potential immunotherapy target for GC. Meanwhile, LAMA/CD44 pair may be a potential adverse indicator for immunotherapy and tumor prognosis.

**Keywords** Gastric cancer, Spatial transcriptome, Single cell RNA sequencing, Immunotherapy, CCL28-CCR10, LAMA/CD44

## Introduction

At present, the incidence and mortality rate of gastric cancer (GC) are relatively high worldwide, which seriously threatens the life expenditure and quality of human life. According to Global Cancer Statistics 2020 [1], the incidence rate ranks fifth and the mortality ranks fourth, which is at a high level in all tumors. The vast majority of GC patients are already in the advanced stage when discovered. Currently, common treatment strategies such as surgery, radiotherapy, and chemotherapy have little efficacy for advanced gastric cancer (AGC) patients. With the improvement of our understanding of the tumor microenvironment (TME), immunotherapy is gradually emerging, greatly improving the survival rate and time of patients with AGC. In 2021, the Food and Drug Administration (FDA) officially approved the combination of nivolumab and chemotherapy for first-line treatment of advanced or metastatic GC, gastroesophageal junction, and esophageal adenocarcinoma patients. This is the first FDA approved first-line immunotherapy for gastric cancer and an important milestone in advanced GC immunotherapy. The immune escape of tumor cells is one of the important mechanisms of GC pathogenesis. Programmed death factor ligand 1 (PD-L1) expressed on tumor cells binds to PD-1 on activated T lymphocytes to provide inhibitory signals, induce T cell apoptosis, and thereby suppress immune response. Immune checkpoint inhibitors (ICIs) such as PD-1/PD-L1 inhibitors specifically block the interaction between the two, enhance the immune activity of T cells, inhibit tumor immune escape, and kill tumor cells. The high expression of PD-L1 in GC tissue provides a possibility for ICIs to be used for the treatment of advanced GC. However, not all patients can benefit from immunotherapy, which attracted our attention. Why do some patients benefit while others do not? Is it due to the different tumor immune microenvironment (TIME)? If the principles and mechanisms can be found, it will greatly help to improve the treatment efficacy of AGC patients.

TME refers to the internal environment in which tumors occur and live, including not only the tumor cells themselves, but also various cells closely related to tumor cells, such as fibroblasts, immune and inflammatory cells, glial cells, etc [2]. In the past decade or so, the mechanism of immune cells in controlling the occurrence and development of cancer has gradually become clear. The role of T cells in tumor immune monitoring has been widely studied, but there is relatively little research on B cells. In recent years, some studies have found that B cells play a huge role in anti-tumor immunity, and their presence and function can be an important factor in cancer prognosis [3]. B cells are a type of cell with the ability to secrete antibodies, derived from multifunctional stem cells in the bone marrow. On the one hand, B cells stimulated by antigens will proliferate and differentiate into a large number of plasma cells, secrete antibodies and circulate in the blood, indirectly exercising their functions through antibody mediated cytotoxicity (ADCC). On the other hand, as an antigen presenting cell (APC), B cells can directly activate T cells and macrophages, which is particularly prominent in the TME. In tumor areas infiltrated by plasma cells, even in small quantities, a large number of cytokines and antibodies can be produced, driving ADCC and phagocytosis, complement activation, and enhancing the antigen presentation of dendritic cells (DC), promoting tumor immunity [4].

In our study, single-cell RNA sequencing (scRNA-seq) and spatial transcriptomics (ST) sequencing techniques were used to investigate the immune landscape of tumor tissue in GC patients and found its correlation with B cells. However, the functional of B cells in tumors is still unclear, especially in the GC microenvironment. The communication between cancer cells and immune elements is a determining factor for tumor progression or regression. In addition, the influence of tumor infiltrating lymphocytes (TIL) on tumor growth and treatment response is becoming increasingly evident. Many studies have focused on the role of T cell response in antitumor immunity, and little is known about the role of B cells in solid tumors. This study provides a detailed analysis of the infiltrating B cell status and tumor cell characteristics of GC. The spatial co-localization of B cells and tumor cells further reveals the potential therapeutic value of the signal axis targeting B cells and tumor cells. We also found that targeting CCL28 may promote the therapeutic effect of PD1 monoclonal antibody, and the

LAMA-CD44 score may have unique clinical immunotherapy predictive value.

## Materials and methods

### Gene expression and clinical data acquisition

In total, gene expression profiles of GC tissues and normal adjacent tissues were obtained from the Cancer Genome Atlas, TCGA-STAD (n = 373) database, and 9 public Gene Expression Omnibus (GEO) datasets GSE84437 (n = 357), GSE115821 (n = 37), GSE126044 (n = 16), GSE135222 (n = 27), GSE179351 (n = 54), GSE19860 (n = 40), GSE35640 (n = 65), GSE78220 (n = 28), and GSE79691 (n = 10), respectively. The metaGSE cohort was combined from all GEO datasets. The single cell and the spatial transcriptome profiles were obtained from OMIX001073 [5] and GSE203612, respectively. The gene expression profiles with immunotherapy information were obtained from 12 published datasets, including Nathanso cohort (n = 24) [6], CheckMate (n = 250) [7], and IMvigor210 (n = 298) [8]. All data analyzed during this study are freely available in previous publications or the public domain all bulk-seq datasets were converted to transcripts per million (TPM) format and corrected for batch effects using the "combat" function of the "sva" package. Prior to analysis, all data were log-transformed.

### Single-cell RNA sequencing (scRNA-seq) data processing

Single-cell RNA sequence (scRNA-seq) data from OMIX001073 [5] cohorts were obtained in the study. We created Seurat objects for total and individual cell types belonging to the scRNA-seq gene expression matrix using the R package "Seurat", then ScaleData and RunPCA functions were performed to obtain the number of principal components (PC) based on the Seurat objects. We used uniform manifold approximation and projection (UMAP) dimensionality reduction to further summarize the top principal components. Finally, with the annotated information for each cell in GC supported by the previous article [9, 10], the Idents and Dimplot functions were used to annotate and visualize the cells of the major TME cell types or subtypes. The FindMarkers function was used to list the markers of each cluster of each cell type in GC, with selection parameters including logFc.threshold = 1, min.pct = 0.25, only.pos = T. Based on these marker genes among different TME cell types, the "clusterprofiler" R package was used to detect Kyoto Encyclopedia of Genes and Genomes (KEGG) pathway database, and gene sets with adjusted p-value < 0.05 were considered significantly enriched. The Cellchat R package was used to calculate the interaction strength of cell–cell communication, and further calculate the L/R signal scores through Lmean + Rmean, representing the average expression value of ligand genes plus receptor gene expression value. In addition, the PAGA, and Slingshot methods in SCP R package were applied to reconstruct the differentiation trajectories and infer cell differentiation states. Furthermore, the pySCENIC package, a Python-based implementation of the SCENIC pipeline was used to investigate the gene regulatory network of transcription factors (TFs) in GC. Furthermore, the 'SCP' R package was used during the data visualization process.

### Spatial transcriptomics data analysis

To explore the spatial specific immune microenvironment in tumor tissue, we employed 10 × Genomics spatial transcriptome (ST) technology in GSE203612 [11] cohort, which the tissues were collected from 19 fresh primary untreated patient tumors immediately after surgery, with 9 cancer types, including carcinoma of the ovarian cancer (OVCA), uterine corpus endometrial carcinoma (UCEC), breast invasive carcinoma (BRCA), prostate adenocarcinoma (PRAD), kidney clear cell carcinoma (KIRC), liver hepatocellular carcinoma (LIHC), colon adenocarcinoma (COAD) and pancreatic ductal adenocarcinoma (PDAC), as well as gastrointestinal stromal tumor (GIST).

### Multiplex immunofluorescence staining and imaging

We collected section from paraffin-embedded tissues of human gastric cancer and peritumor from Cancer Center, Union Hospital, Tongji Medical College, Huazhong University of Science and Technology. Multiplex immunofluorescence (mIF) analysis was performed for detection of EPCAM, CCL28, CCR10, and CD138. All the images were captured using a Leica DM 2500 microscope.

### Establishment of animal models and flow cytometry

To verify our hypothesis in vivo, we constructed subcutaneous tumor models using two cell lines, the mouse gastric cancer MFC cell line and the mouse colon cancer MC38 cell line, on 615 mice (n = 24) and C57 mice (n = 24), respectively. The shCCL28 cell line was transfected with lentivirus and inoculated (CCL28-1 F:CCGGGCTGTCATCCTTCATGTTAAACTCGAGTTTAACATGAAGGATGACAGCTTTTTG; R:AATTCAAAAAGCTGTCATCCTTCATGTTAAACTCGAGTTTAACATGAAGGATGACAGC; CCL28-2 F:CCGGCCCGCACAATCGTACTTTGAACTCGAGTTCAAAGTACGATTGTGCGGGTTTTTG;R:AATTCAAAAACCCGCACAATCGTACTTTGAACTCGAGTTCAAAGTACGATTGTGCGGG; CCL28-3 F:CCGGCTGAGGTGTCTCATCATGTTTCTCGAGAAACATGATGAGACACCTCAGTTTTTG;R:AATTCAAAAACTGAGGTGTCTCATCATGTTTCTCGAGAAACATGATGAGACACC

TCAG). The experiment was divided into four groups: IgG group, shCCL28 group, anti PD-L1 group, and shCCL28 + anti PD-L1 (Comb) group, with 6 mice in each group. Each mouse was inoculated with 3×10^5 tumor cells, then the size and weight of the tumor were measured. Further, flow cytometry was used to observe the TME, we detected the extracellular (CD45, CD3, CD4, CD8, CD19, CD20, CD11b, CD11c, F4/80, CD86, and NK1.1) and intracellular indicators (CD206, GZMB, and IFNγ), respectively.

#### Related in vitro experiments

Besides, the effects of CCL28 gene on MFC and MC38 tumor cells were verified through relevant in vitro experiments, including cell proliferation experiment, colony formation assay, cell cycle checkpoint detection, apoptosis flow cytometry, and cell invasion and migration experiment, the experiment was conducted according to previously published protocols [12].

#### Detection of CCL28

Collect CTRL and shCCL28 cell culture supernatant for CCL28 detection. According to the instructions for using the FineTest CCL28 ELISA kit (EM1932), take the kit at room temperature. Add 100 μL diluted standard and test sample, 100 μL Detection Reagent A, 100 μL Detection Reagent B, 90 μL Substrate Solution, and 50 μL Stop Solution to each hole in sequence, and finally measure the absorbance using an enzyme-linked immunosorbent assay (ELISA) reader.

#### Statistical analysis

R software (version 4.1.3) was used for statistical analysis and draw charts. Correlations between two continuous variables were assessed via spearman's correlation coefficients. The Chi-square test and student's-t test were used for categorical variables and continuous variables, respectively. The "survminer" package was used to determine the optimal cut-off value. Cox regression and Kaplan–Meier analyses were performed via the survival package. All tests performed were two sided, and P values < 0.05 indicated statistically significant (* meant p value < 0.05, ** meant p value < 0.01, *** meant p value < 0.001, **** meant p value < 0.0001, ns meant p value > 0.05).

## Results

#### Spatial transcriptomic revealed B cell aggregation around tumor cells in various tumor microenvironments

Re-analysis of various tumor spatial transcriptome (ST) data, including breast invasive carcinoma (BRCA), gastrointestinal stromal tumor (GIST), liver hepatocellular carcinoma (LIHC), ovarian cancer (OVCA), pancreatic ductal adenocarcinoma (PDCA), and uterine corpus endometrial carcinoma (UCEC), we found that B cell aggregation typically existed in the tumor microenvironment (TME), and the proximity of the B cell population to tumor cells indicated crosstalk between B cells and tumor cells. As shown in Fig. 1A and sFig.1A,B, the B cells identified in BRCA sections were very close to the tumor cells in spatial distribution, and the IgG and IgA antibody genes in cancer samples had similar abundance, which was similar to the literature reports [13]. While in GIST, the expression of IgA gene was dominant (Fig. 1B), in OVCA, the secretion of IgG antibodies was dominant (Fig. 1C), in PDCA, the abundance of B cells identified was low (Fig. 1D), in UCEC, the secretion of IgG antibodies was dominant (Fig. 1E), and in LIHC, rich expression of IgG antibody genes was observed (sFig.1D) [14, 15].

#### ScRNA-seq landscape of infiltrating B cell subsets in GC

To generate a thorough transcriptional atlas of B cells in GC, we first reanalyzed the public scRNA profiles of 166,533 cells from 10 GC patients in a previous study [5] and identified 12 distinct clusters, including T cells & NK cells (98809), myloid cells (6572), B cells (16247), mast cells (2896), erythrocytes (69), B cells (plasma cells) (6201), epithelial cells (20535), endothelial cells (2911), endocrine cells (1843), fibroblasts (3111), and smooth muscle cells (1424) (Fig. 2A). After further subcluster analysis by extracting all B cells and plasma cells, we identified naïve_B cells in $CD20^{+}$cells, germinal center B cells (GC_B cells), memory_B cells, and at the same time, a group of plasma_cells expressed CD138 were also identified (Fig. 2B). Being consistent with a previous report [16], naïve_B cells were characterized by the specific expression of PRPSAP2, MYO1E, ELL3, LRMP, and RGS13, GC_B cells were characterized by YBX3, IL4R, TCL1A, FCER2, and IGHD, memory_B cells were characterized by LDLRAD4, NR4A2, TNFRSF13B, AIM2, CD27, whereas plasma_cells specifically expressed the markers of JCHAIN, FKBP11, DERL3, MZB1, SDC1, SUGCT (Fig. 2C). As shown in the bar chart (Fig. 2D), compared to peripheral blood, the TME infiltrates more plasma cells. However, it is interesting that GC_B cells are almost exclusively present in the TME, indicating the presence of a very small number of tertiary lymphoid structures (TLS) in the GC microenvironment, which is consistent with previous reports [17, 18].

#### Antibody class switching to IgA in the GC tumor microenvironment

The distribution of plasma cells and antibody isotypes in the GC TME was not yet clear, therefore, we further analyzed the plasma cell infiltration status of GC patients. Principal component analysis (PCA) was used

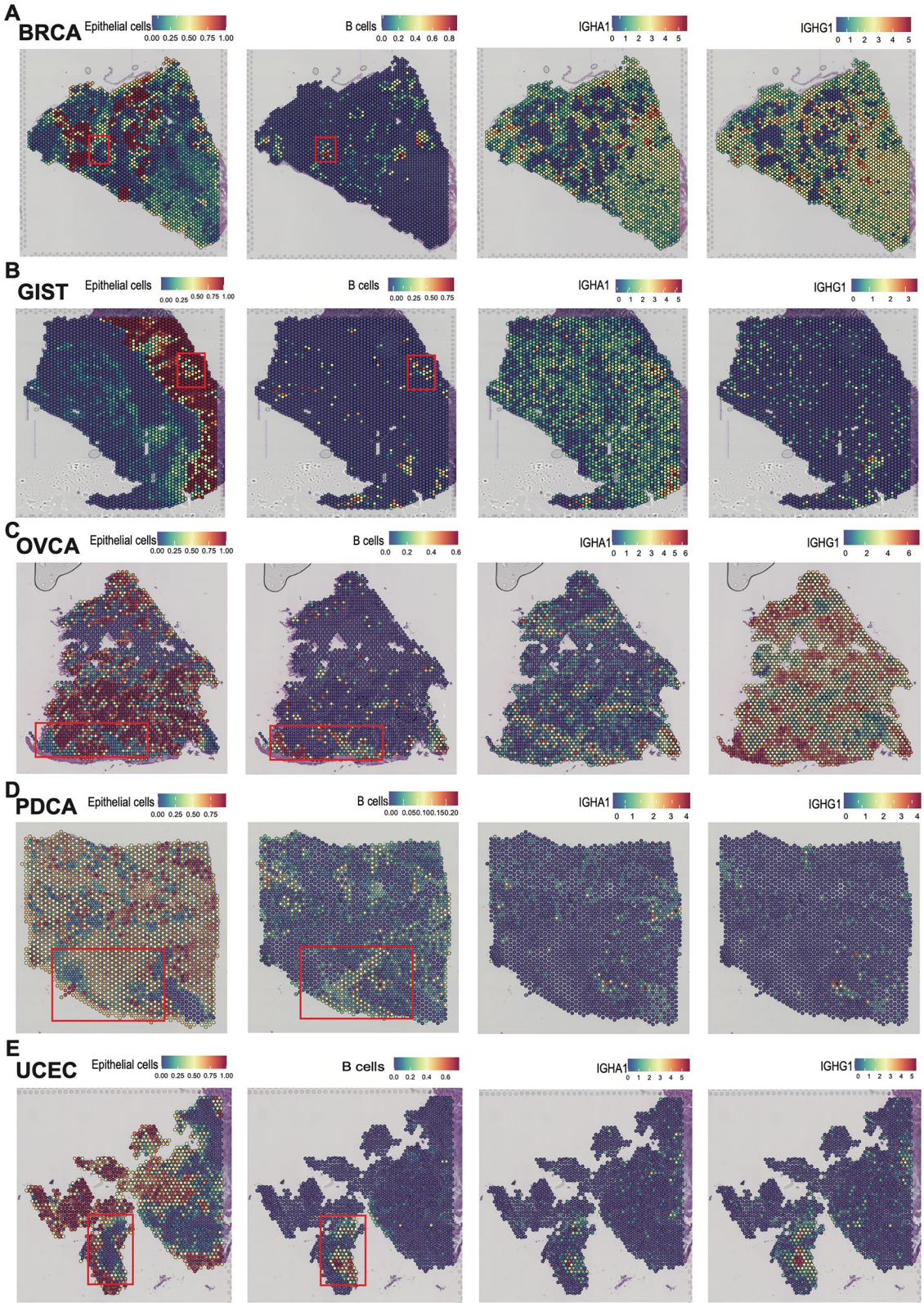


**Fig. 1** Spatial distribution of B cells in various tumor immune microenvironments and their relationship with regional tumor epithelium. **A**-**E** the spatial distribution of tumor epithelial cells, B cells, IgA, and IgG antibody genes in BRCA (**A**), GIST (**B**), OVCA (**C**), PDCA (**D**), UCEC (**E**)

for dimensionality reduction based on antibody genes. We observed that cells with high expression of IGHG or IGHA constituted almost all principal components (PC), and there was overlap in cells with multiple IgA subtypes [19] (sFig.2D). The scatter plot also showed significant differences between the two cell types (Fig. 2E), which indicated that IgA PC was the main PC type for GC. Similarly, from the results of bulk RNA-seq, we found that the expression levels of IgA related genes (IGHA1, IGHA2) in tumor samples were higher than those of IgG related genes (IGHG1, IGHG3, and IGHG4) (sFig.2A). To further explore its functional characteristics, cells with high IGHG and low IGHA expression were defined as IgG PC, while cells with low IGHG and high IGHA expression were defined as IgA PC (Fig. 2F–G, sFig.2B, C). Among them, IgA PCs were mainly involved in the regulation of phagocytic pathways, such as phagocytosis, and engulfment, while IgG PCs were associated with B cell immune response and MHC class I antigen presentation, such as regulation of B cell activation, indicated that IgG PCs might be more likely to participate in anti-tumor immune regulation, and IgA PCs might be more involved in promoting tumor immunity [20]. To investigate the effects of IgA and IgG PC on cancer progression and patient survival, we analyzed the correlation between plasma cell infiltration and patient prognosis in the TCGA-STAD cohort. The results showed that the higher the abundance of IgA infiltration, the shorter the patient's survival time. However, IgG plasma cells did not show any correlation with prognosis (sFig.3B). Surprisingly, the bar graph shows that there are no more IgA plasma cells in the GC TME than in the surrounding and peripheral blood, indicating that IgA PC in the GC microenvironment mainly comes from the periphery. Therefore, tumor cells may recruit IgA PC through certain signaling pathways (Fig. 2G). Therefore, we analyzed the cellular relationship between B cells and tumor cells in the GC microenvironment, and the results showed that CCL28 is mainly expressed by tumor cells, while CCR10 is mainly expressed in plasma cells as shown in Fig. 2H, which might be one of the mechanisms underlying the abundance of IgA PCs in the GC microenvironment. The multiple immunofluorescence (mIF) also validated the CCL28-CCR10 axis difference between immune therapy responder (R) and non-responder (NR) (Fig. 2I, sFig.2E). Therefore, targeting the CCL28-CCR10 axis may be one of the potential targets for enhancing immunotherapeutic efficacy in GC. Through patient samples underwent immunotherapy, it was found that CCL28 mainly originated from tumor epithelial cells, while CCR10 and CD138 were co-located. At the same time, patients with high expression of CCL28 had more $CD138^{+}$cells and a shorter survival time, while patients with low expression of CCL28 had a longer survival time.

### Gastric cancer infiltrating $CD20^{+}$B cells exhibited two unique differentiation trajectories

In order to further analyze the subtype status of B cells infiltrating in gastric cancer, we identified five B cell clusters by extracting all $CD20^{+}$B cells for further subcluster analysis, including B_cells_C1_RGS13, B_cells_C2_TCL1A, B_cells_C3_CD99, B_cells_C4_GPR183, and B_cells_C5_NR4A1 (Fig. 3A). For example, B_cells_C1_RGS13 were mainly associated with aerobic respiration, B_cells_C2_TCL1A were mainly associated with B cell activation, B_cells_C3_CD99 were mainly associated with cytoplasmic translation, B_cells_C4_GPR183 were mainly associated with regulation of lymphocyte proliferation, and B_cells_C5_NR4A1 were mainly associated with intrinsic apoptotic signaling pathway (sFig.4A-E). Figure 3B showed the corresponding markers of each cluster. The bar chart showed that compared to peripheral blood, gastric cancer microenvironment infiltrates more C1, C4, and C5 (Fig. 3C). Furthermore, we determined the possible involvement of regulons in all five cluster B cells by single-cell regulatory network inference and clustering (SCENIC) analysis (Fig. 3D), to determine the changes in transcription factors (TFs) during B cell differentiation.(C1: CUX1 [21], H2AFY [22], MYBL1 [23], ZNF236 [24], SMARCA4 [25]; C4: FOXO3 [26], ZFHX2 [27], RXRA [28], RXRB [29], GRHL2 [30], TGIF1 [31]). At the same time, the unique state of C1-C5 B cells was also displayed in the functional enrichment analysis (Fig. 3I, sFig.4F). In pseudotime analysis, we found that C1 cells were located at the beginning of the cell trajectory, while C4 and C5 were located at the end, respectively (Fig. 3E-G). Figure 3H showed high abundance of TGFb expression in GC infiltrating B cells, while C4

(See figure on next page.)

**Fig. 2** B cell profiles of immune microenvironment in human gastric cancer. **A** Unified manifold approximation and projection (UMAP) of 166,533 single cells from 10 patients, colored by main cell types. **B** Umap plot of B cells. **C** Bubble plot showing the expression of marker genes in major B cell subpopulations. **D** Histography of the different B cells components in each tissue. **E** Scatter plot showing the independent cell distribution based on the expression of IgG and IgA. **F** Bubble plot showing the expression of marker genes in major plasma cell subpopulations. **G** Histography of the different plasma cells components in each tissue. **H** Umap plot showing the gene expression of CCL28 (Up) and CCR10 (Down). **I** The mIF showed the expression levels of EPCAM, CCL28, CCR10, and CD138 in NR (PFS = 2.07 m, up) and R (PFS = 11.1 m, down)

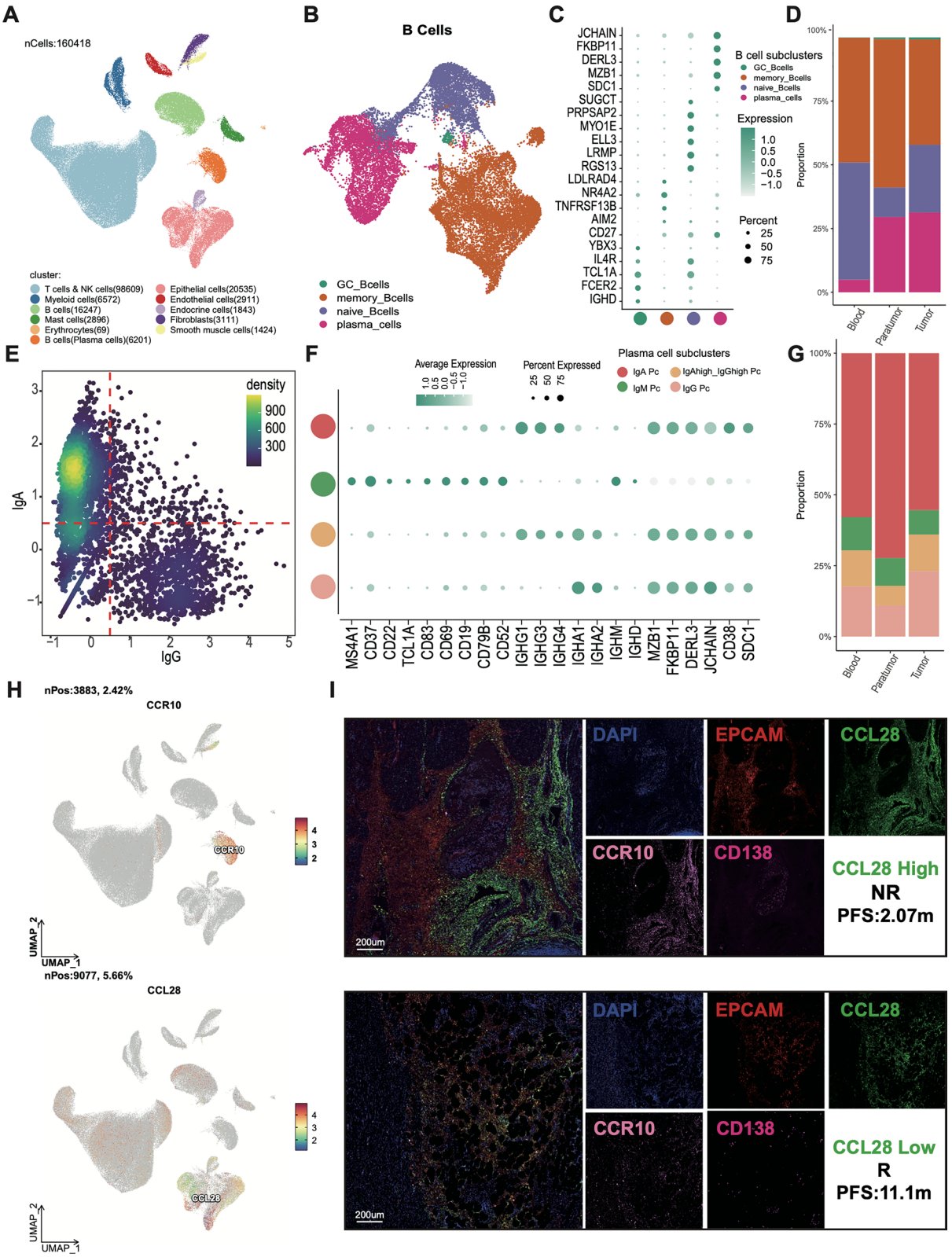


**Fig. 2** (See legend on previous page.)

cells in the terminal differentiation state expressed IL-10, and C5 cells secreted IL-35, further suggesting that GC infiltrating B cells gradually evolved into B cells in different immunosuppressive states. Previous studies have reported the detection of Breg cells in the peripheral blood of GC, which were immunosuppressive cells characterized by IL-10, IL-35, TGFb, and PD1, thereby promoting tumor progression [32, 33]. Interestingly, cells exhibited high expression of NR4A1, NR4A2, ZFP35, and EGF1 in lineage 2, which was not present in lineage 1, indicated differences in the function of $CD20^{+}$B cells with two different lineages. For example, lineage 2 is associated with response to amphetamine, fat cell differentiation, response to amine, interleukin production, T cell differentiation, etc. (Fig. 3I). These data indicated that GC infiltrating $CD20^{+}$B cells had unique immunosuppressive functions and important subtypes that affect the effectiveness of immunotherapy.

#### Identification of seven tumor cell states

Due to the high heterogeneity of tumor cells, we conducted non-negative matrix factorization (NMF) analysis, and identified a total of 40 metagenes that were preferentially co-expressed by subpopulations of malignant cells across tumors. Then, hierarchical clustering was used to characterize these 40 metagenes into gene expression signatures, and high concordance was shown among their signatures (Fig. 4A, B). Seven tumor cell states, including Cell Cycle (140), WH (1258), Metal (1560), OP (727), Interferon (159), Epi_dif2 (2711), and Epi_dif1 (2650) in GC were identified and used to assess the intrinsic functional characteristics of tumor cells (Fig. 4C–K). The tumor cells in different states were found to be involved in different regulatory functions (Fig. 4M). For example, Cell-Cycle cells were mainly associated with chromosome segregation, WH cells were mainly associated with regulation of leukocyte migration, Metal cells were mainly associated with cellular transition metal ion homeostasis, OP cells were mainly associated with oxidative phosphorylation, Epi_dif1 cells were mainly associated with MHC protein complex assembly, Epi_dif2 cells were mainly associated with response to virus. Additionally, it is worth noting that interferon-like tumor cells were found to be involved in adaptive immune response. Then, we evaluated the impact of different tumor cell states on patient survival (sFig.5A-H). In the non-immunotherapy TCGA-STAD cohort (n = 373), high expression of Epi-dif1 ($P = 0.026$), and cell cycle ($P = 0.054$) were associated with better OS, while low expression of Wh ($P = 0.0049$), interferon ($P = 0.056$), OP ($P = 0.19$), Epi-dif2 ($P = 0.015$), and OS ($P = 0.013$) were associated with better OS.

#### Crosstalk landscape between tumor cells and B cells

Next, we studied the communication between all cells. Generally, fibroblasts and smooth muscle cells (SMC) in stromal cells, and myeloid cells and T cells&NK cells in immune cells were usually the strongest signal senders and receivers, respectively (sFig.6A). B cells and plasma cells were more likely to receive signals from stromal cells and send them to T cells and myeloid cells [2, 3] (sFig.6B), which indicated B cells and plasma cells might be an important immune mediator regulating intercellular communication in the TME of GC.

When analyzing the pathway between tumor cells and B cells-based L/R pair, ADGRE5, APP, and macrophage migration inhibitory factor (MIF) signaling pathways were the most significant enrichment pathways (Fig. 5A, sFig.6C,D). We further found that the ADGRE5 signaling pathway was mainly enriched in tumor cells, rather than in B cells. In the MIF signaling pathway, tumor cells were the main output cells, especially interferon like tumor cells, which were also the main signal cells in all pathways, while B cells were the main receiving cells (sFig.6C). In summary, these data indicated that the communication mode between tumor cells and B cells dynamically changed with the progression of GC.

The L/R pairs of MIF/(CD74, CD44, or CXCR4) and APP/CD74 were the most prominent interactions involved in signal transduction from tumor cells to B cells (Fig. 5A, B). Some studies have reported the tumor promoting effects of MIF and APP, and their potential association with B cells may explain other mechanisms of tumor progression [34–36]. Some L/R pairs mediated signal transduction from tumor cells to B cells, while others mediated signal transduction from B cells to tumor

(See figure on next page.)

**Fig. 3** Human gastric cancer $CD20^{+}$B cells exhibit two unique differentiation trajectories. **A** UMAP visualization of 14,536 $CD20^{+}$B cells across 10 cancer patients. **B** Bubble plot showing the expression of tag genes between B cells clusters. **C** Histography of the different B cells components in each tissue. **D** Regulons enriched in each B cell cluster detected via pySCENIC analysis. **E–H** Developmental trajectory of B cells in five different states inferred by PAGA **(E)** and Slingshot **(F)**, colored by Lineage1 and Lineage2 **(G)**. The UMAP plots showed the expression levels of IL10, IL12A, TGFB1, and EBI3 genes in $CD20^{+}$B cells **(H)**. The scale represents the predictive differentiation trajectory. The higher value represents the degree of differentiation. **I** Heatmap display of the expression of highly variable genes (left) and GO, KEGG pathway functional enrichment (right) along the pseudotime of the Lineage1 trajectory and the Lineage2 trajectory

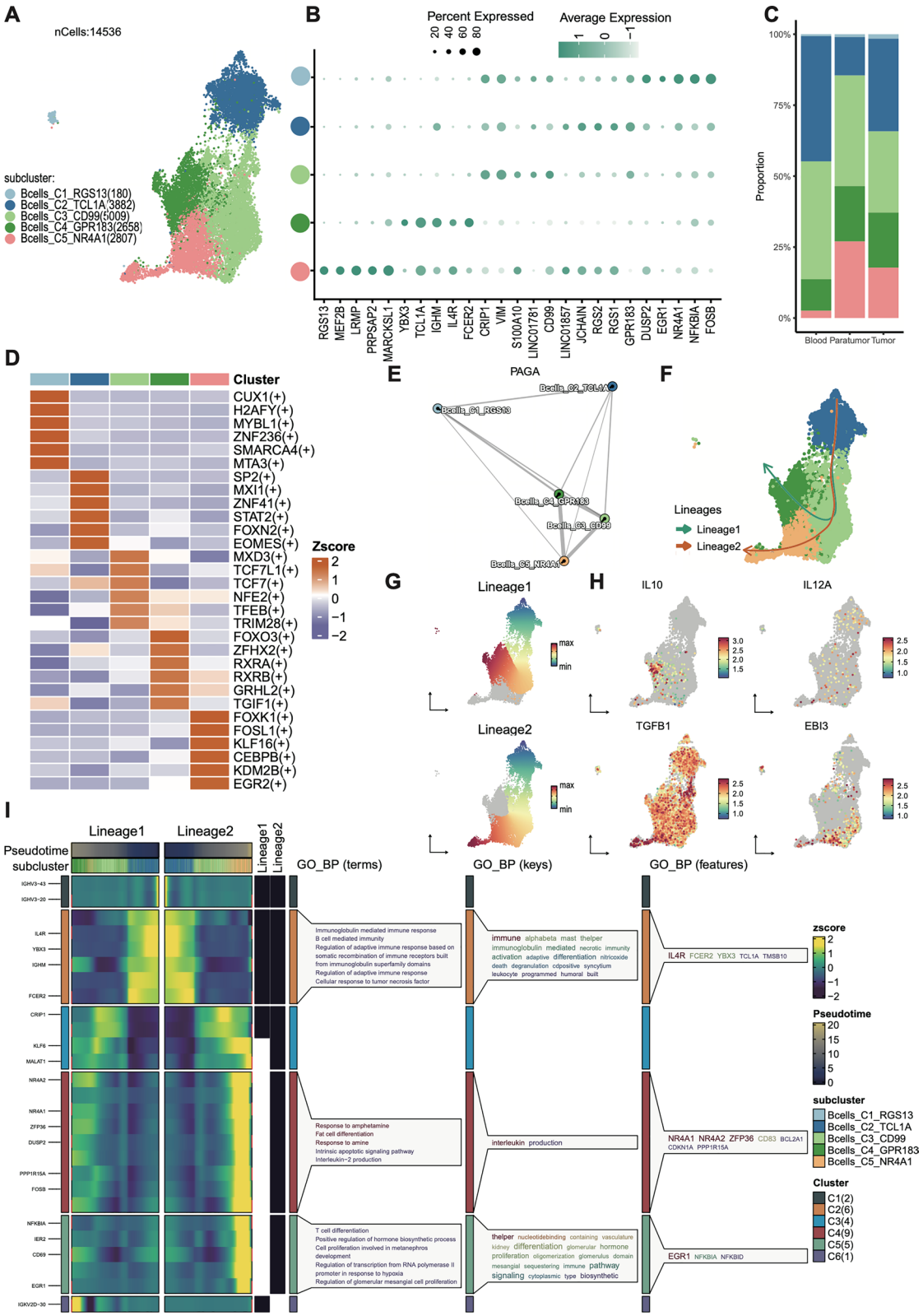


**Fig. 3** (See legend on previous page.)

cells, such as MDK/SDC1 [37, 38]. In addition, further research was conducted on the expression levels of 81 L/R pairs involved in significant communication between tumor cells and PC. In the TCGA-STAD cohort, 41 molecules were differentially expressed between tumor and normal samples (FDR < 0.05), of which 35.1% were upregulated in tumor samples (Fig. 5C). In the GSE84437 cohort [39], 25 molecules were differentially expressed between peritoneal metastatic and non-metastatic samples (FDR < 0.05), of which 24% were upregulated in peritoneal metastasis samples (Fig. 5D). In the IMvigor210 cohort treated with anti PD-L1 [8], 15 molecules were differentially expressed in both treatment responsive and non-responsive patients, but only 1% of the molecules were upregulated in responsive patients (Fig. 5E). These data suggested that B-cell signal perturbations may significantly affect the response of cancer patients to immunotherapy. Therefore, we speculated that global crosstalk between tumor cells and PC might promote cancer development and be associated with adverse reactions to immune checkpoint blockade (ICB) treatment. In order to further select reliable L/R pairs between tumor cells and B cells, we evaluated their expression levels in tissue slices using ST data analysis. Based on the expression and biological localization analysis of L/R pairs, we identified four pairs of L/R pairs (LAMA3/CD44, MDK/SDC1 (Fig. 5F), CCL28/CCR10, and GDF/TGFBR2 (sFig.7A,B)) with high reliability between tumor cells and B cells and these L/Rs were also observed in tumor epithelial cells and B cells (Fig. 5G, H).

#### LAMA-CD44 crosstalk between GC cells and B cells is a potential predictive marker for immunotherapy and tumor prognosis

To analyze the clinical value of B cell and tumor cell crosstalk, we calculated a score based on 37 L/R pairs and then conducted a univariate COX regression analysis based on average value of receptor gene expression (GeneRmean) and ligand gene expression (GeneLmean). As shown in Fig. 6E (left), in Nathanso cohorts (n = 24), the crosstalk of LAMA (LAMA3/5), LAMB (LAMB2/3), LAMC (LAMC1/2), and CD44 was associated with poor prognosis of GC, with most of them were significant ($P < 0.05$). Both L/R pairs were associated with poor prognosis, indicated that the relationship between tumor epithelial cells and B cells in GC microenvironment might be related to promoting tumor progression. Also, in two large immunotherapy cohorts (CheckMate (n = 250), and IMvigor210 (n = 298)), LAMA/CD44 pairs were associated with poor prognosis. Therefore, we further calculated the AUC values of these L/R pairs for predicting immunotherapy effects in nine immunotherapy cohorts, including GSE115821, GSE126044, GSE135222, GSE179351, GSE19860, GSE35640, GSE78220, GSE79691, and Nathanso cohort (Fig. 6A (right)). LAMA/CD44 pairs had a higher AUC value (average 0.7), indicated that the LAMA/CD44 axis might be a potential immunotherapy prediction marker for GC immunotherapy. LAMA/CD44 in the TCGA-STAD cohort was also associated with poor disease-free survival (DFS) ($P = 0.026$), and in multiple immunotherapy cohorts, LAMA/CD44 pair was also associated with poor OS.

To explore the immune status reflected by the LAMA/CD44 score, we analyzed the relationship between the LAMA/CD44 score and immune modulators. As results shown in Fig. 6G, high LAMA/CD44 score suggested higher levels of immune infiltrating cells and immune modulators, indicated that high LAMA/CD44 was a relatively immunosuppressive microenvironment. The combination of LAMA/CD44 blockers and immunotherapy might be a new treatment method for GC. Subsequently, in GSE7961 ($P = 0.067$), GSE19860 ($P = 0.013$), CheckMate cohorts ($P = 0.072$), Nathanso cohorts ($P = 0.038$), and IMvigor210 cohorts ($P = 0.016$), compared to immunotherapy non-responders (NR), immunotherapy responders (R) had lower LAMA/CD44 scores (Fig. 6H-M). These data indicated that LAMA/CD44 had the potential to become a unique prognostic factor for clinical immunotherapy.

#### Targeting CCL28 significantly inhibited tumor growth, activated TIME, and enhanced anti-PDL1 effect

The specific expression of CCL28 in tumor epithelial cells may be a unique potential target, in order to verify that targeting CCL28 can synergistically enhance the efficacy of immunotherapy, we conducted in vivo and in vitro experiments. In the experiment, we used two cell lines, the mouse gastric cancer MFC cell line and the mouse colon cancer MC38 cell line. The shCCL28 cell line was

(See figure on next page.)

**Fig. 4** Seven unique subtypes were identified in human gastric cancer epithelial cells. **A** Heatmap depicts pairwise correlations of 40 intra-tumoral programs derived from ten tumors. Clustering identifies seven coherent expression programs across tumors. **B** UMAP visualization of the 7 tumor cell states. **C**-**J** 7 epithelial (tumor) cell state scores calculated by the AUCell R package. **K** The CNV scores (left) and tumor score (right) were different among cells of the six tumor cell states. **M** Heatmap display of differential genes (left) and GO, KEGG pathway functional enrichment (right) in 7 tumor transcriptional states

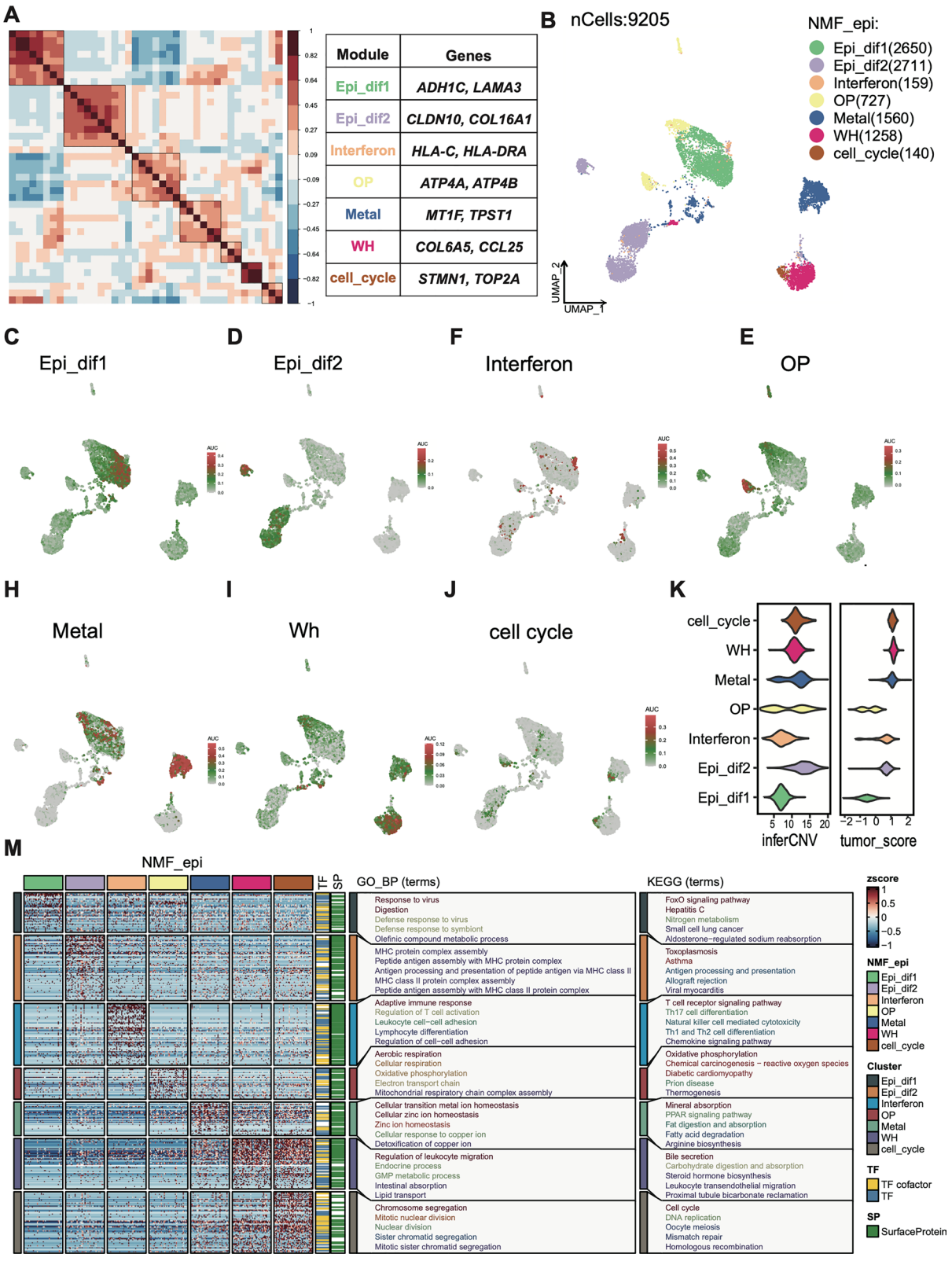


**Fig. 4** (See legend on previous page.)

transfected with lentivirus on both MFC and MC38 cells. In vitro experiments, we conducted cell proliferation experiment, colony formation assay, cell cycle checkpoint detection, apoptosis flow cytometry, and cell invasion and migration experiment (sFig.7). However, there were no statistical differences in all results, which confirmed that inhibiting CCL28 alone did not work in vitro, and it was speculated that it may work within TME. Therefore, we conducted relevant in vivo experiments. We constructed subcutaneous tumor models using MFC and MC38 tumor cells on 615 mice (n = 24) and C57BL/6 J mice (n = 24), respectively. The experiment was divided into four groups: IgG group, shCCL28 group, anti PD-L1 group, and shCCL28 + anti PD-L1 (Comb) group, with 6 mice in each group. Each mouse was inoculated with $1 \times 10^6$ tumor cells and the size of the tumor was measured. Finally, we took the photographs of the tumor, a statistical map of the tumor weight, and a growth curve (Fig. 7A–G, J–M). We performed flow cytometry on tumor tissue to detect the infiltration and function of B, $CD3^+$T, $CD8^+$T, $CD4^+$T, $IFN^+CD8^+$T, $GZMB^+CD8^+$T, MDSC and DC (Fig. 7H, I, sFig.8, sFig.9C, D). The above results showed that knocking down CCL28 can significantly promote immune cell infiltration and enhance the therapeutic effect of anti PD-L1. To sum up, through cell experiments, we have demonstrated that CCL28 alone does not work in vitro, suggesting that it may play a role in TME. Then, tumor cells were implanted into mice, by analyzing the tumor volume, weight and overall survival rate, we found that knock down CCL28 can significantly inhibit tumor growth, this effect is amplified when combined with anti PD-L1. Further, FASC indicated that targeting CCL28 can significantly promote the infiltration and function of $CD8^+$T cell by regulating B cell function, and has the ability to synergize immunotherapy.

## Discussion

In recent years, with the rise of immunotherapy, the survival of tumor patients has been greatly improved. Gastric cancer is a malignant tumor with high incidence rate and mortality rate worldwide. Due to the slow progression of the disease, GC rarely presents early symptoms, with over 70% of patients developing advanced diseases, while the five-year survival rate of patients with AGC is only 6%. At present, in the first-line treatment of advanced gastric cancer, immunotherapy has become a consensus [40–42]. However, not all AGC patients can benefit from immunotherapy. It is necessary to explore the potential mechanisms and powerful biomarkers to predict the efficacy and prognosis of tumor immunotherapy.

Tumor infiltrating T cells and B cells are necessary and synergistic components in TME. However, current research mainly focuses on T cells, and their role in tumor immune monitoring has been widely studied. The mechanism of controlling the occurrence and development of tumors is gradually becoming clear, but there is relatively little research on B cells, which makes their roles in different types of cancer controversial. In this study, we systematically and comprehensively plotted the transcriptional characteristics of gastric cancer infiltrating B cells by deciphering their single-cell transcriptomics and spatial transcriptomics.

By using ST data, we explored the spatial-specific immune microenvironment in tumor tissues, all data were obtained from public cohorts in the GEO database. By analyzing scRNA and ST profiles, we found that B cells and tumor cells have certain co-localization in various cancer species, such as breast invasive carcinoma (BRCA), gastrointestinal stromal tumor (GIST), ovarian cancer (OVCA), pancreatic ductal adenocarcinoma (PDCA), and uterine corpus endometrial carcinoma (UCEC), which has the significance of further studying the interaction between B cells and tumor cells. Therefore, based on scRNA and ST sequence analysis, this study explores relevant scientific issues and elucidates the research potential of targeting B cells and clinical transformation, laying a solid theoretical foundation for clinical research.

Our findings align with previous studies indicating that B cells play significant roles in the TIME [43]. However, the infiltration and function of B cells vary in different types of cancer. The presence and behavior of B cells in the tumor microenvironment can affect tumor progression and patient prognosis. In some cancers, such as breast cancer and lung cancer, B cells inhibit tumor growth by secreting antibodies, neutralizing tumor

(See figure on next page.)

**Fig. 5** Crosstalk in cellular communication between gastric cancer cells and B cells. **A**-**B** Crosstalk pattern diagram showing signaling from tumor cells to B and plasma cells and from B and plasma cells to tumor cells. The internal heatmap shows the communication probability of the selected L/R pair crosstalk between tumor cells of 7 different states and 4 types of B cells and 4 types of plasma cells. The differentially expressed L/R pairs between tumor and normal samples from the TCGA-STAD cohort are marked in red, those between samples from R versus NR patients from IMvigor210 are marked in green, and those in both cohorts are marked in dark green. **C**-**E** Bubble plots showing the change in the expression of L/R pairs between tumor and normal samples from the TCGA-STAD cohort (**C**), GSE84437 (**D**) and IMvigor210 cohort (**E**). Pie chart (right) showing the ratio of upregulated to downregulated molecules in the two groups. **F** The expression of selected genes in tissue sections. **G**, **H** The selected genes expression of 11 main cell types and 7 tumor cell states

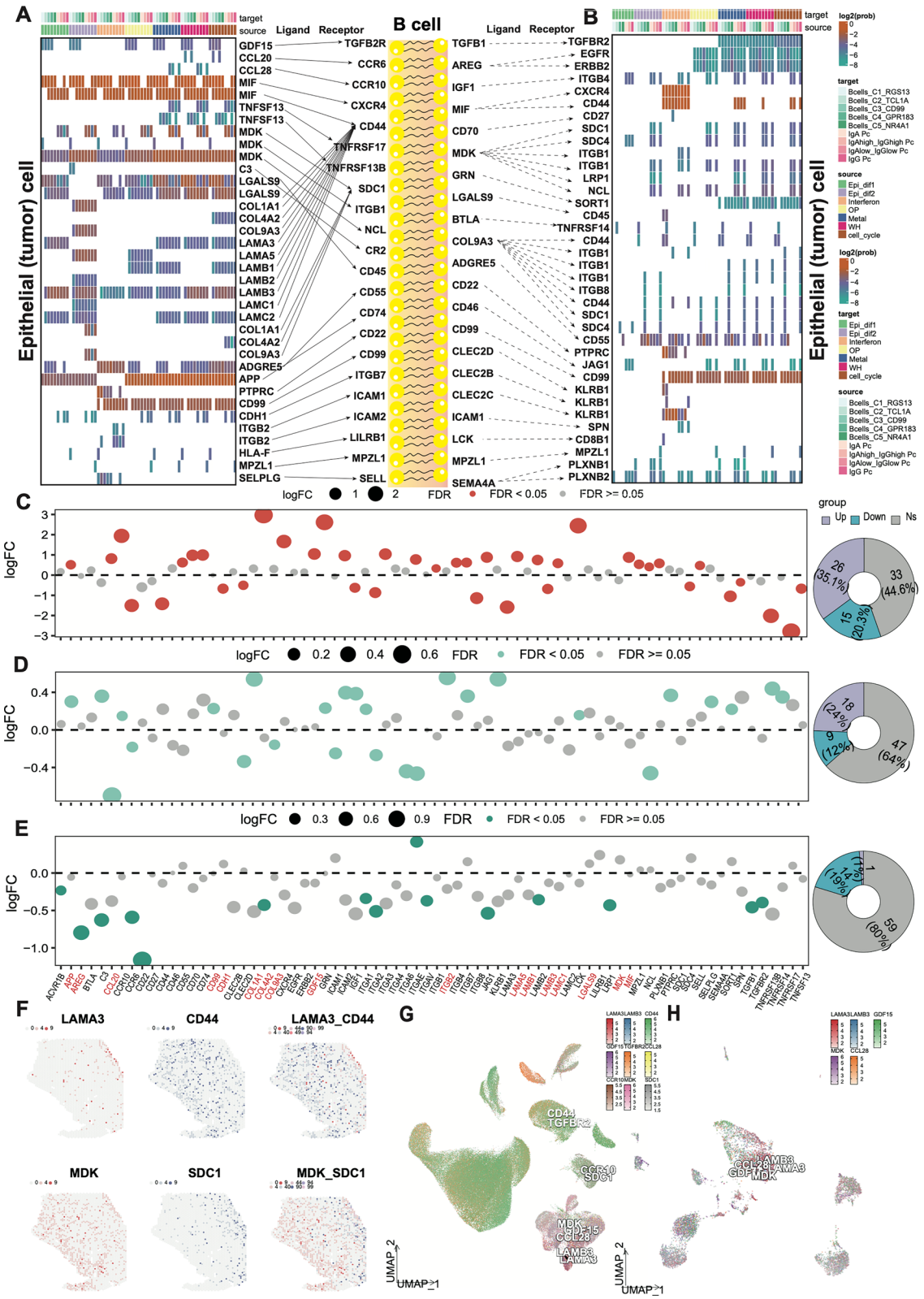


**Fig. 5** (See legend on previous page.)

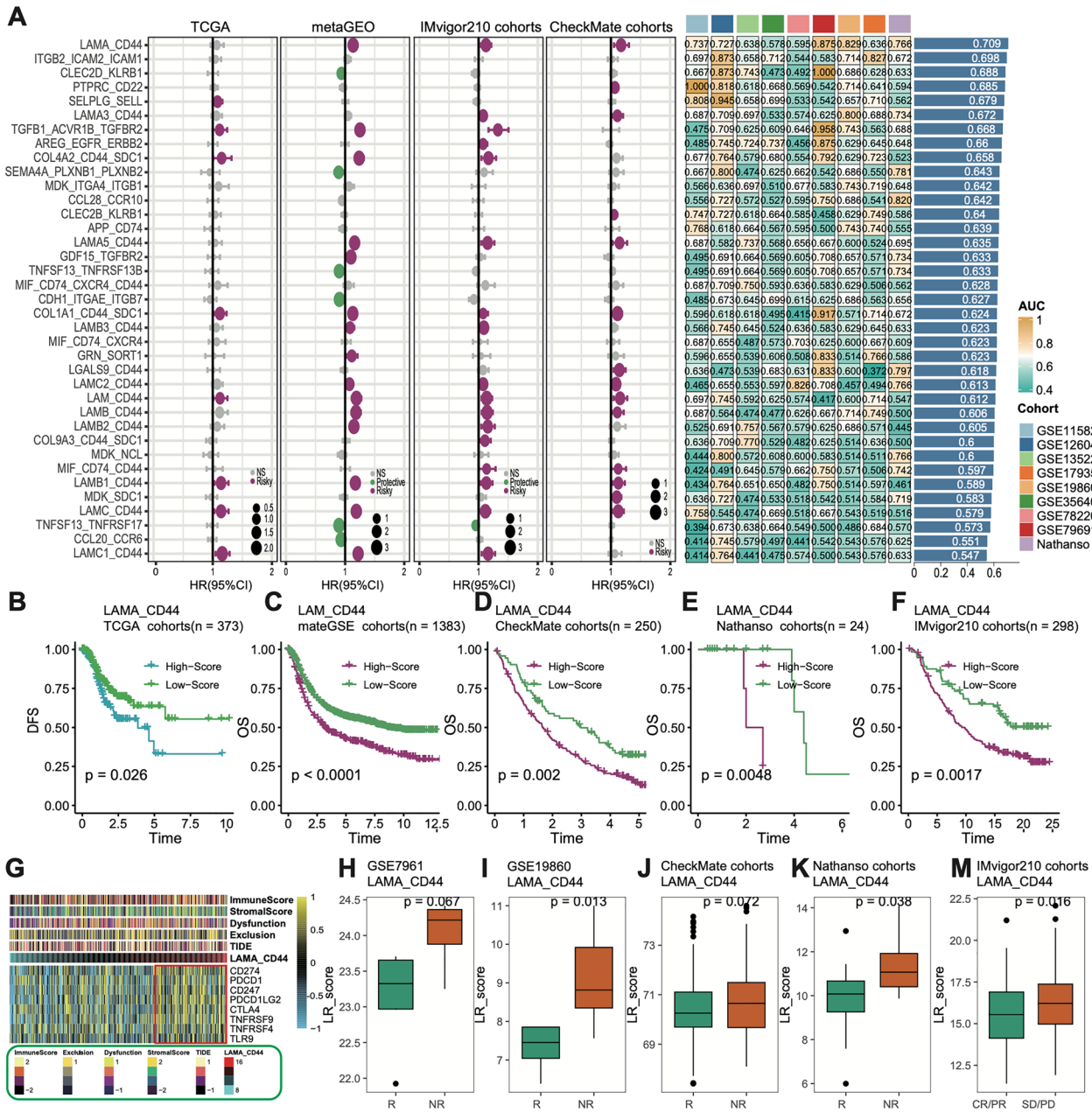


**Fig. 6** LAMA-CD44 crosstalk between GC cells and B cells is a potential predictive marker for immunotherapy and tumor prognosis. **A** Forest plot (left) showing the hazard ratio (HR) of 37 L/R pairs based on stepwise Cox regression analysis. Heat map (right) displays a score based on 37 L/R pairs to predict the corresponding AUC values of immunotherapy across 8 immunotherapy cohorts. **B** Kaplan–Meier curves of DFS according to the LAMA-CD44 pair score in TCGA-STAD cohort. **C**-**F** Kaplan–Meier curves of OS according to the LAMA-CD44 pair score in mateGSE cohorts (**C**), checkmate cohorts (**D**), Nathanso cohorts (**E**), and IMvigor210 cohorts (**F**). **G** Heatmap showing the correlation between LAMA-CD44 pair score and immune checkpoint molecules. (H-M) The distribution of LAMA-CD44 pair score between R and NR of immunotherapy in GSE7961 (**H**), GSE19860 (**I**), CheckMate cohorts (**J**), Nathanso cohorts (**K**) and IMvigor210 cohorts (**M**)

antigens, promoting anti-tumor immune response, and activating T cells, helping to improve the prognosis of patients [44, 45]. In other cancers, such as gastric cancer and colorectal cancer, specific subgroups of B cells such as regulatory B cells (Breg) and IgA secreting cells may inhibit T cell activity, promote tumor growth and metastasis, and lead to poor prognosis by secreting immunosuppressive cytokines (such as IL-10) [46, 47]. Therefore, understanding the mechanism of action of B cells in specific tumor types is of great significance for developing

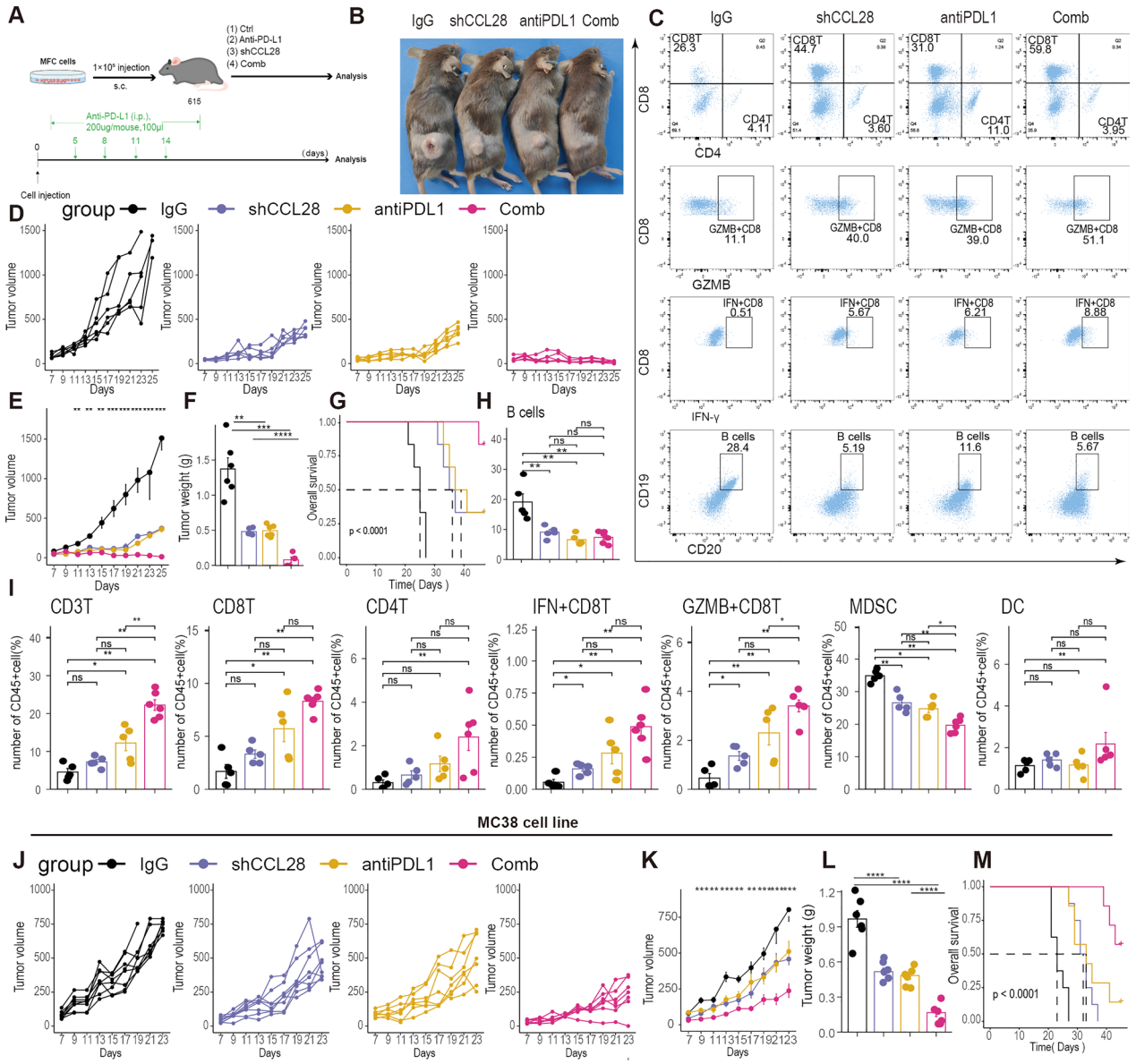


**Fig. 7** Inhibiting CCL28 can promote the inhibition of tumor progression and the effectiveness of immunotherapy. **A-I** 615 mice were implanted with $1 \times 10^6$ MFC cells and received (1) IgG isotype control (IgG); (2) shCCL28, (3) PD-L1 mAb, or (4) shCCL28 plus PD-L1 mAb (Comb). A schematic view of the treatment plan **(A)**, tumor image **(B)**, tumor volume **(D**, **E)**, weight **(F)**, and overall survival **(G)** were measured every 2 days, n = 6 mice per group. **C** Representative diagram of flow cytometry. **H**, **I** The percentages of tumor-infiltrating B, $CD3^+T$, $CD8^+T$, $CD4^+T$, $IFN^+CD8^+T$, $GZMB^+CD8^+T$, MDSC and DC were analyzed by flow cytometry. n = 5–6/group. **J-M** The tumor volume **(J**, **K)**, weight **(L)**, and overall survival **(M)** of MC38 cell line in vivo

tumor therapies targeting B cells. By regulating the function or specific subgroups of B cells, new strategies and potential for cancer immunotherapy can be provided. Consistent with these studies, our data indicate abundant IgA plasma cell infiltration in the GC TIME. Additionally, we confirmed the recruitment of $CCR10^+IgA$ plasma cells by tumor-secreted CCL28, a mechanism previously suggested but not extensively validated in GC. In gastric cancer, we found that tumor cells can secrete chemokine CCL28, which can attract IgA positive plasma cells expressing CCR10. The enrichment of these $CCR10^+IgA^+$plasma cells in the tumor microenvironment is closely related to poor prognosis of patients. IgA positive plasma cells may inhibit anti-tumor immune responses by secreting immunosuppressive cytokines, thereby promoting tumor progression and metastasis.

Despite these advancements, several questions remain unresolved. The study's limitations include a relatively small sample size and the need for multi-center data to validate the prediction model. Furthermore, no prospective randomized clinical trials (RCTs) have been conducted to confirm these findings. The mechanisms underlying the interaction between GC cells and B cells require deeper exploration. Future research should focus on large-scale studies to validate these results, conduct RCTs to confirm the therapeutic potential of targeting CCL28, and investigate the detailed molecular mechanisms of B cell and tumor cell interactions.

The role of B cells in the tumor microenvironment is complex and multifaceted. Understanding the mechanism of action of B cells in specific tumor types is of great significance for developing tumor therapies targeting B cells. B cell targeted therapy has shown great potential in cancer treatment. By blocking specific signaling pathways, such as CCL28/CCR10, anti-tumor immune responses can be significantly activated, enhancing the efficacy of PD-L1 monoclonal antibodies. In addition, combining with other targeted therapies such as blocking the LAMA/CD44 signaling pathway may further improve the prognosis of gastric cancer and other cancer patients. Future research should focus on large-scale studies and clinical trials to validate the efficacy and safety of these strategies, in order to provide more effective treatment options for cancer patients.

## Conclusion

To sum up, in our study, we identified a significant amount of crosstalk between GC cells and B cells through scRNA-seq and ST-seq analyses, revealing two differentiation trajectories of GC B cells, which tended to be inhibitory B cell states with IL-10 and IL-35 terminal states. And by analyzing the L/R pairs, we creatively found that the expression of LAMA/CD44 signal axis is a predictive marker for immunotherapy and tumor prognosis. Animal experiments also confirmed that targeting CCL28 can significantly promote immune cell infiltration and enhance the therapeutic effect of anti PD-L1. The combination of LAMA/CD44 or CCL28/CCR10 blockers and PD-1/PD-L1 may be a new treatment for GC.

**Abbreviations**

| | |
|---|---|
| GC | Gastric cancer |
| AGC | Advanced gastric cancer |
| TME | Tumor microenvironment |
| TIME | Tumor immune microenvironment |
| NGS | Next-generation sequencing technology |
| scRNA-seq | Single-cell RNA sequencing |
| ST | Spatial transcriptome |
| IHC | Immunohistochemistry |
| mIF | Multiple immunofluorescence |
| TIL | Tumor infiltrating lymphocytes |
| L/R | Ligand/receptor |
| TCGA | The cancer genome Atlas |
| GEO | Gene expression omnibus |
| BRCA | Breast invasive carcinoma |
| GIST | Gastrointestinal stromal tumor |
| LIHC | Liver hepatocellular carcinoma |
| OVCA | Ovarian cancer |
| PDCA | Pancreatic ductal adenocarcinoma |
| UCEC | Uterine corpus endometrial carcinoma |
| GC_B cells | Germinal center B cells |
| TLS | Tertiary lymphoid structures |
| PCA | Principal component analysis |
| PC | Principal component |
| R | Responder |
| NR | Non-responder |
| SCENIC | Single-cell regulatory network inference and clustering |
| TF | Transcription factor |
| NMF | Non-negative matrix factorization |
| SMC | Smooth muscle cells |
| MIF | Migration inhibitory factor |
| ICBs | Immune checkpoint blockades |
| DFS | Disease-free survival |
| ADCC | Antibody-dependent cell-mediated cytotoxicity |
| APC | Antigen presenting cell |
| DC | Dendritic cells |
| RCT | Randomized clinical trials |

## Supplementary Information

The online version contains supplementary material available at https://doi.org/10.1186/s12967-024-05606-9.

Additional file 1: **Supplementary Figure 1. Spatial transcriptomics explained the distribution characteristics of marker genes in various types of cancer epithelium and B cells**.Epcam, MS4A1, SDC1 gene expression in multiple cancers, including BRCA, GIST, LIHC, OVCA, PDCA, and UCEC.

Additional file 2: **Supplementary Figure 2. Single cell landscape of human gastric cancer plasma cells.** Box plots showing the expression levels of IgA and IgG related genes.Uniform manifold approximation and projectionof 5518 cells from 10 patients, colored by major cell types. Violin plot showing the expression of antibody-relatedgenes in subclusters of plasma cells.UMAP visualization of antibody-related genes expression showing IgG and IgA cells are the dominated PCs based on dimension reduction of PCA with selected gene.the immunofluorescence quantitative bar chart of CD138 cell, $CCR10^{+}$/$CD138^{+}$ cell and $CCL28^{+}$/$EPCAM^{+}$ cell.

Additional file 3: **Supplementary Figure 3. The correlation between plasma cells and clinical practice.**The histogram shows the significantly enriched pathways of plasma cell clusters, including IgA Pc, IgG Pc, IgA high_IgG high Pc, and IgA low_IgG low Pc. The survival curves show the relationship between plasma cell infiltration levels and prognosis in four Pc groups.

Additional file 4: **Supplementary Figure 4. Functional enrichment and trajectory analysis of gastric cancer B cells.**The histogram shows the significantly enriched pathways of B cell clusters. Gaussian process regression curves with a 95% confidence interval showing the dynamic expression of TCL1A, NR4A1, CD99 and GPR183 along the pseudotime of the Lineage1 trajectoryand the Lineage2 trajectory.

Additional file 5: **Supplementary Figure 5. Correlation between epithelial transcription status and clinical prognosis in gastric cancer.** KM plots of seven tumor epithelial cell states, including Epi-dif1, Wh, cell cycle, interferon, OP, Epi-dif2, unknown, and Metal.

Additional file 6: **Supplementary Figure 6. Disturbance of communication between various cells in the gastric cancer microenvironment.**Crosstalk networks show B cells tend to send signals to T&NK cells and myeloid cells but receive signals from stromal cells. Dot plot shows the incoming and outgoing signal strength in different cell types. Dot plots show the incoming and outgoing interaction strength

of tumor cell states in all signaling pathways, MK/MIF signaling, ADGRE5/CD55 signaling and APP/CD74 signaling.Heat map shows the signaling pathways enriched by each tumor cell states in both incoming and outgoing signaling patterns.

Additional file 7: **Supplementary Figure 7. Related cell phenotype experiments on MFC and MC38 tumor cells.**The line chart showed no statistical difference in OD valuesbetween shCCL28 and shNC on both MFC and MC38 cells. ELISA showed a decrease in protein levels of CCL28 in MFC-shCCL28 and MC38-shCCL28 cell lines, respectively. The colony formation graphand corresponding bar graphshowed that there was no statistical difference in clone formation between shCCL28 and shNC on both MFC and MC38 cells.Cell cycle checkpoint detection showed no difference in the percentage of G2 between MFC and MC38 cells. Flow cytometry showed no statistically significant difference in the apoptotic effects of shCCL28 and shNC on MFC and MC38 cells. Cell invasion and migration experiments showed no statistical differences between shCCL28 and shNC on MFC and MC38 cells.

Additional file 8: **Supplementary Figure 8. Gating strategies for flow cytometry in specific immunity and innate immunity, respectively.**

Additional file 9: **Supplementary Figure 9. Inhibiting CCL28 can promote the inhibition of tumor progression and the effectiveness of immunotherapy.** C57BL/6J mice were implanted with $1\times10^6$ MC38 cells and received treatment as 615 mice.A schematic view of the treatment plan.Tumor image, tumors were measured every 2 days, n=6 mice per group.Representative diagram of flow cytometry.The percentages of tumor-infiltrating B, $CD3^+$T, $CD8^+$T, $CD4^+$T, $IFN^+CD8^+$T, $GZMB^+CD8^+$T, MDSC and DC were analyzed by flow cytometry. n=6-8/group.

**Acknowledgements**
We are grateful to the researchers who provided the original data.

**Author contributions**
(I) Conception and design: CS Zheng and XF Dai; (II) Administrative support: XF Dai; (III) Provision of study materials or patients:X Cai, JR Yang and YS Guo; (IV) Collection and assembly of data: X Cai and YC Yu; (V) Data analysis and interpretation: X Cai and JR Yang; (VI) Manuscript writing: JR Yang; (VII) Final approval of manuscript: All authors.

**Funding**
This work was supported by the National Natural Science Foundation of China (No. 82072041 and No. 82372069).

**Availability data and materials**
Publicly available datasets were analyzed in this study. Public data used in this work can be acquired from the TCGA repository (http://cancergenome.nih.gov/), and Gene Expression Omnibus (GEO, https://www.ncbi.nlm.nih.gov/geo/).

## Declarations

**Ethics approval and consent to participate**
The Ethics Committee of the Union Hospital, Tongji Medical College, Huazhong University of Science and Technology and Institutional Animal Care and Use Committee, Huazhong University of Science and Technology granted approval for the study (No. 2014-041, and No. IACUC [2023] 3525).

**Competing interests**
All authors have completed the ICMJE uniform disclosure form. The authors have no competing of interest to declare.

**Author details**
[1]Cancer Center, Union Hospital, Tongji Medical College, Huazhong University of Science and Technology, Wuhan 430022, People's Republic of China. [2]Institute of Radiation Oncology, Union Hospital, Tongji Medical College, Huazhong University of Science and Technology, Wuhan 430022, People's Republic of China. [3]Department of Radiology, Union Hospital, Tongji Medical College, Huazhong University of Science and Technology, Wuhan 430022, People's Republic of China. [4]Hubei Key Laboratory of Molecular Imaging, Wuhan 430022, People's Republic of China. [5]Department of Urology, Union Hospital, Tongji Medical College, Huazhong University of Science and Technology, Wuhan 430022, People's Republic of China. [6]Present Address: Department of Radiation and Medical Oncology, Zhongnan Hospital of Wuhan University, Wuhan 430071, People's Republic of China.

Received: 11 February 2024 Accepted: 14 August 2024
Published online: 30 August 2024

**References**

1. Global Cancer Statistics. GLOBOCAN estimates of incidence and mortality worldwide for 36 cancers in 185 countries - pubmed. Cancer Journal for Clinicians: Published online; 2020. p. 2020.
2. Downs-Canner SM, Meier J, Vincent BG, Serody JS. B cell function in the tumor microenvironment. Annu Rev Immunol. 2022;40:169–93. https://doi.org/10.1146/annurev-immunol-101220-015603.
3. Zhang E, Ding C, Li S, et al. Roles and mechanisms of tumour-infiltrating B cells in human cancer: a new force in immunotherapy. Biomark Res. 2023;11(1):28. https://doi.org/10.1186/s40364-023-00460-1.
4. Wei Y. B cell heterogeneity, plasticity, and functional diversity in cancer microenvironments. Oncogene: Published online; 2021.
5. Sun K, Xu R, Ma F, et al. scRNA-seq of gastric tumor shows complex intercellular interaction with an alternative T cell exhaustion trajectory. Nat Commun. 2022;13(1):4943. https://doi.org/10.1038/s41467-022-32627-z.
6. Nathanson T, Ahuja A, Rubinsteyn A, et al. Somatic mutations and neoepitope homology in melanomas treated with CTLA-4 blockade. Cancer Immunol Res. 2017;5(1):84–91. https://doi.org/10.1158/2326-6066.CIR-16-0019.
7. Braun DA, Hou Y, Bakouny Z, et al. Interplay of somatic alterations and immune infiltration modulates response to PD-1 blockade in advanced clear cell renal cell carcinoma. Nat Med. 2020;26(6):909–18. https://doi.org/10.1038/s41591-020-0839-y.
8. Mariathasan S, Turley SJ, Nickles D, et al. TGFβ attenuates tumour response to PD-L1 blockade by contributing to exclusion of T cells. Nature. 2018;554(7693):544–8. https://doi.org/10.1038/nature25501.
9. Luo H, Xia X, Huang LB, et al. Pan-cancer single-cell analysis reveals the heterogeneity and plasticity of cancer-associated fibroblasts in the tumor microenvironment. Nat Commun. 2022;13(1):6619. https://doi.org/10.1038/s41467-022-34395-2.
10. Li X, Sun Z, Peng G, et al. Single-cell RNA sequencing reveals a pro-invasive cancer-associated fibroblast subgroup associated with poor clinical outcomes in patients with gastric cancer. Theranostics. 2022;12(2):620–38. https://doi.org/10.7150/thno.60540.
11. Barkley D, Moncada R, Pour M, et al. Cancer cell states recur across tumor types and form specific interactions with the tumor microenvironment. Nat Genet. 2022;54(8):1192–201. https://doi.org/10.1038/s41588-022-01141-9.
12. Zhang B, Li J, Hua Q, et al. Tumor CEMIP drives immune evasion of colorectal cancer via MHC-I internalization and degradation. J Immunother Cancer. 2023;11(1): e005592. https://doi.org/10.1136/jitc-2022-005592.
13. Long F. The potential crosstalk between tumor and plasma cells and its association with clinical outcome and immunotherapy response in bladder cancer. J Trans Med. 2023. https://doi.org/10.1186/s12967-023-04151-1.
14. Wei Y, Lao XM, Xiao X, et al. Plasma cell polarization to the immunoglobulin G phenotype in hepatocellular carcinomas involves epigenetic alterations and promotes hepatoma progression in mice. Gastroenterology. 2019;156(6):1890-1904.e16. https://doi.org/10.1053/j.gastro.2019.01.250.
15. Wu RQ, Lao XM, Chen DP, et al. Immune checkpoint therapy-elicited sialylation of IgG antibodies impairs antitumorigenic type I interferon responses in hepatocellular carcinoma. Immunity. 2023;56(1):180-192.e11. https://doi.org/10.1016/j.immuni.2022.11.014.
16. Hamish WK, Nara O, John CR, Andrew JC, Gary W, Sarah AT, Louisa KJ. Single-cell analysis of human B cell maturation predicts how antibody class switching shapes selection dynamics. Sci Immunol. 2021. https://doi.org/10.1126/sciimmunol.abe6291.

17. Li Z, Jiang Y, Li B, et al. Development and validation of a machine learning model for detection and classification of tertiary lymphoid structures in gastrointestinal cancers. JAMA Netw Open. 2023;6(1): e2252553. https://doi.org/10.1001/jamanetworkopen.2022.52553.
18. Yin YX, Ling YH, Wei XL, et al. Impact of mature tertiary lymphoid structures on prognosis and therapeutic response of Epstein-Barr virus-associated gastric cancer patients. Front Immunol. 2022;13: 973085. https://doi.org/10.3389/fimmu.2022.973085.
19. Patil NS, Nabet BY, Müller S, et al. Intratumoral plasma cells predict outcomes to PD-L1 blockade in non-small cell lung cancer. Cancer Cell. 2022;40(3):289-300.e4. https://doi.org/10.1016/j.ccell.2022.02.002.
20. Meylan M, Petitprez F, Becht E, et al. Tertiary lymphoid structures generate and propagate anti-tumor antibody-producing plasma cells in renal cell cancer. Immunity. 2022;55(3):527-541.e5. https://doi.org/10.1016/j.immuni.2022.02.001.
21. Liu N, Sun Q, Wan L, et al. CUX1, a controversial player in tumor development. Front Oncol. 2020;10:738. https://doi.org/10.3389/fonc.2020.00738.
22. Huang Y, Huang S, Ma L, et al. Exploring the prognostic value, immune implication and biological function of H2AFY gene in hepatocellular carcinoma. Front Immunol. 2021;12: 723293. https://doi.org/10.3389/fimmu.2021.723293.
23. Zhu J, Wu Y, Yu Y, Li Y, Shen J, Zhang R. MYBL1 induces transcriptional activation of ANGPT2 to promote tumor angiogenesis and confer sorafenib resistance in human hepatocellular carcinoma. Cell Death Dis. 2022;13(8):727. https://doi.org/10.1038/s41419-022-05180-2.
24. Halama N, Yard-Breedijk A, Vardarli I, et al. The Kruppel-like zinc-finger gene ZNF236 is alternatively spliced and excluded as susceptibility gene for diabetic nephropathy. Genomics. 2003;82(3):406–11. https://doi.org/10.1016/s0888-7543(03)00120-4.
25. Tian Y, Xu L, Li X, Li H, Zhao M. SMARCA4: current status and future perspectives in non-small-cell lung cancer. Cancer Lett. 2023;554: 216022. https://doi.org/10.1016/j.canlet.2022.216022.
26. Lin Z, Niu Y, Wan A, et al. RNA m6 A methylation regulates sorafenib resistance in liver cancer through FOXO3-mediated autophagy. EMBO J. 2020;39(12): e103181. https://doi.org/10.15252/embj.2019103181.
27. Habib AM, Matsuyama A, Okorokov AL, et al. A novel human pain insensitivity disorder caused by a point mutation in ZFHX2. Brain. 2018;141(2):365–76. https://doi.org/10.1093/brain/awx326.
28. Di Martino O, Ferris MA, Hadwiger G, et al. RXRA DT448/9PP generates a dominant active variant capable of inducing maturation in acute myeloid leukemia cells. Haematologica. 2022;107(2):417–26. https://doi.org/10.3324/haematol.2021.278603.
29. Chano T, Kita H, Avnet S, Lemma S, Baldini N. Prominent role of RAB39A-RXRB axis in cancer development and stemness. Oncotarget. 2018;9(11):9852–66. https://doi.org/10.18632/oncotarget.23955.
30. Wang Z, Coban B, Wu H, et al. GRHL2-controlled gene expression networks in luminal breast cancer. Cell Commun Signal. 2023;21(1):15. https://doi.org/10.1186/s12964-022-01029-5.
31. Razzaque MS, Atfi A. TGIF1-Twist1 axis in pancreatic ductal adenocarcinoma. Comput Struct Biotechnol J. 2020;18:2568–72. https://doi.org/10.1016/j.csbj.2020.09.023.
32. Rosser EC, Mauri C. Regulatory B cells: origin, phenotype, and function. Immunity. 2015;42(4):607–12. https://doi.org/10.1016/j.immuni.2015.04.005.
33. Sarvaria A, Madrigal JA, Saudemont A. B cell regulation in cancer and anti-tumor immunity. Cell Mol Immunol. 2017;14(8):662–74. https://doi.org/10.1038/cmi.2017.35.
34. Klemke L, De Oliveira T, Witt D, et al. Hsp90-stabilized MIF supports tumor progression via macrophage recruitment and angiogenesis in colorectal cancer. Cell Death Dis. 2021;12(2):155. https://doi.org/10.1038/s41419-021-03426-z.
35. Sumaiya K, Langford D, Natarajaseenivasan K, Shanmughapriya S. Macrophage migration inhibitory factor (MIF): a multifaceted cytokine regulated by genetic and physiological strategies. Pharmacol Ther. 2022;233: 108024. https://doi.org/10.1016/j.pharmthera.2021.108024.
36. Lee HN, Jeong MS, Jang SB. Molecular characteristics of amyloid precursor protein (APP) and its effects in cancer. Int J Mol Sci. 2021;22(9):4999. https://doi.org/10.3390/ijms22094999.
37. Hu XF, Yao J, Gao SG, Yang YT, Peng XQ, Feng XS. Midkine and syndecan-1 levels correlate with the progression of malignant gastric cardiac adenocarcinoma. Mol Med Rep. 2014;10(3):1409–15. https://doi.org/10.3892/mmr.2014.2369.
38. Akgun H, Metintas S, Ak G, et al. Prognostic value of midkine, syndecan-1, hyaluronan synthase-2, sestrin-1, laminin subunit alpha-4 and fibulin-3 for malignant pleural mesothelioma. Arch Med Sci. 2023;19(2):355–64. https://doi.org/10.5114/aoms/112525.
39. Yoon SJ, Park J, Shin Y, et al. Deconvolution of diffuse gastric cancer and the suppression of CD34 on the BALB/c nude mice model. BMC Cancer. 2020;20(1):314. https://doi.org/10.1186/s12885-020-06814-4.
40. Janjigian YY, Shitara K, Moehler M, et al. First-line nivolumab plus chemotherapy versus chemotherapy alone for advanced gastric, gastro-oesophageal junction, and oesophageal adenocarcinoma (CheckMate 649): a randomised, open-label, phase 3 trial. Lancet. 2021;398(10294):27–40. https://doi.org/10.1016/S0140-6736(21)00797-2.
41. Kang YK, Chen LT, Ryu MH, et al. Nivolumab plus chemotherapy versus placebo plus chemotherapy in patients with HER2-negative, untreated, unresectable advanced or recurrent gastric or gastro-oesophageal junction cancer (ATTRACTION-4): a randomised, multicentre, double-blind, placebo-controlled, phase 3 trial. Lancet Oncol. 2022;23(2):234–47. https://doi.org/10.1016/S1470-2045(21)00692-6.
42. Shitara K, Van Cutsem E, Bang YJ, et al. Efficacy and safety of pembrolizumab or pembrolizumab plus chemotherapy vs chemotherapy alone for patients with first-line, advanced gastric cancer: the keynote-062 phase 3 randomized clinical trial. JAMA Oncol. 2020;6(10):1571–80. https://doi.org/10.1001/jamaoncol.2020.3370.
43. Ma J, Wu Y, Ma L, et al. A blueprint for tumor-infiltrating B cells across human cancers. Science. 2024. https://doi.org/10.1126/science.adj4857.
44. Gu Y, Liu Y, Fu L, et al. Tumor-educated B cells selectively promote breast cancer lymph node metastasis by HSPA4-targeting IgG. Nat Med. 2019;25(2):312–22. https://doi.org/10.1038/s41591-018-0309-y.
45. Hollern DP, Xu N, Thennavan A, et al. B cells and T follicular helper cells mediate response to checkpoint inhibitors in high mutation burden mouse models of breast cancer. Cell. 2019;179(5):1191-1206.e21. https://doi.org/10.1016/j.cell.2019.10.028.
46. Wang Z, Lu Z, Lin S, et al. Leucine-tRNA-synthase-2-expressing B cells contribute to colorectal cancer immunoevasion. Immunity. 2022;55(6):1067-1081.e8. https://doi.org/10.1016/j.immuni.2022.04.017.
47. Overacre-Delgoffe AE, Bumgarner HJ, Cillo AR, et al. Microbiota-specific T follicular helper cells drive tertiary lymphoid structures and anti-tumor immunity against colorectal cancer. Immunity. 2021;54(12):2812-2824.e4. https://doi.org/10.1016/j.immuni.2021.11.003.


## Publisher's Note